Received: 27 September 2020 | Revised: 16 May 2021 | Accepted: 27 June 2021

DOI: 10.1002/stc.2818

RESEARCH ARTICLE

WILEY

Weigh-in-motion of train loads based on measurements of rail strains

Annamaria Pau | **Fabrizio Vestroni**

Department of Structural and Geotechnical Engineering, Sapienza University of Rome, Rome, Italy

Correspondence
Annamaria Pau, Department of Structural and Geotechnical Engineering, Sapienza University of Rome, via Eudossiana 18, 00184 Rome, Italy.
Email: annamaria.pau@uniroma1.it

Funding information
EU, Grant/Award Number: RFCS-2018_800687; Sapienza Research, Grant/Award Numbers: RP1181642D8B9FAF, RM120172B397172A

Summary

This paper deals with the identification of the weight of a train in motion, based on the measurement of the time history of strains at the foot of the rail. The direct problem is initially considered, modelling the rail as a one-dimensional infinite Euler–Bernoulli beam, resting on a viscoelastic soil and subjected to a Dirac delta load travelling at constant speed. A closed-form solution is used to investigate the sensitivity of the response to the main mechanical parameters. Then, the inverse problem consisting of the identification of the loads for a given time history of measured strains is addressed as a minimization problem whose objective function is based on the difference between experimental and model time histories of strains. First, an updating of the interpretative model using the time history of a train of known weight is pursued. Then, the actual load identification is performed. The procedure proposed is initially applied to numerical data, also contaminated by noise. Within the context of a Bayesian approach, identifiability of model parameters and minimum number of measurements is examined; moreover, the sensitivity of parameter estimation to errors in the known load and the sensitivity of load identification to errors in the model parameters are investigated, as well as the effect of noise. A validation is finally performed, using rail strains measured on a stretch of line run by a locomotor of known weight.

KEYWORDS

inverse problems, load identification, rail strains, sensitivity analysis, weigh-in-motion

1 | INTRODUCTION

Knowledge of the dynamic loads acting on a structure is very important for its design, control, diagnosis and maintenance. Increased standards of safety in railway transport require awareness of the loads actually travelling on railway lines, in particular when dealing with freight trains. This enables the timely schedule of maintenance and monitoring of rail wear, as well as to check unbalanced loads that can affect vehicle safety. The achievement of this goal requires the development of methods for the identification of travelling loads. In particular, techniques that identify the forces in motion without disturbing the normal operation process have attracted the interest of researchers over the last few

decades. These techniques enable the vehicle loads to be determined indirectly from the dynamic responses and lead to the formulation of an inverse problem.

The structure can be modelled as an Euler–Bernoulli plane infinite beam with constant properties resting on a viscoelastic foundation subjected to Dirac delta loads travelling at constant speed, whose solution has been known in closed form since the middle of last century.[1–3] This model was successfully used to synthetically describe the response of rocket test tracks[2] and train tracks,[1,4] proving its ability to represent with satisfactory approximation the main physical phenomena tied to the amplification occurring when the travelling load approaches the critical speed. When considering foundations typical of railway engineering applications, the critical velocities obtained using the Euler–Bernoulli beam are almost the same as those from the Timoshenko beam.[5] The effectiveness of the description provided by the Euler–Bernoulli beam was proved experimentally in several papers.[6–8]

Over time, research has advanced to describe more complex cases, in particular, concerning the behaviour of the ballast or the interaction vehicle rail. Some non-exhaustive examples are the Pasternak two-parameter foundation accounting for the interaction between adjacent springs, discussed in previous studies,[9,10] also for Timoshenko beams,[5] as well as investigations of the effect of load intensity and speed on the foundation stiffness, including nonlinear hardening of the ballast,[11] 2-D[12] and 3-D[13,14] descriptions of the elastic foundation, detailed modelling of rails resting on periodic supports,[15] which is relevant when dealing with trains travelling at high speed, or dynamic models representing the interaction of the rail track and the waggon system.[14,16]

Load identification problems, in their broadest sense, may include different characteristics of the load, which are its time history and its distribution in space. Existing load identification methods can be classified into time domain, frequency domain, state space, orthogonal function expansion and neural network methods. As most inverse problems, load identification based on the measured response is an ill-conditioned problem: the response is typically a continuous vector function in the spatial coordinates, which is only known at a few points of the structure and at discrete time instants. Many load identification methods require the application of regularization techniques, one of the most popular of which is Tichonov's, to enhance the accuracy of the solution. The reader can find a broad list of references in previous studies.[17–20] Among the approaches proposed, the dynamic programming is worth mentioning.[20] A large number of methods operate in the time domain and identify moving forces minimizing the difference between measured and model-predicted time-histories of the response. Using laboratory tests, it was shown that time domain methods have the best performance compared to other moving load identification methods, except for the computational time.[21]

Although weigh-in-motion procedures were largely used in bridge structures,[19] their applications to infinite beams such as rails, where vibration modes cannot be defined, are relatively limited; examples of such research can be found in previous studies.[14,22–30] Some authors[23,30] have focused on the identification of the wheel-rail contact force as a tool to detect irregularities. In fact, a number of aspects can influence the wheel-rail contact force such as wheel profile[22] and rail roughness,[29] both tied to rail and wheel wear,[27] horizontal forces that can arise and need to be evaluated to assess the risk of derailment.[25] Commercial high precision weigh-in-motion systems are also available, but they require significant modifications of the track, which has to be supported over sensored sleepers, as well as strict speed limitations.[24] Contemporary research focuses on indirect load identification with measurements of the response, which do not disturb integrity of the rail nor require any costly changes or interruption. This can be done applying on the rail resistive strain gauges,[14,26] piezoelectric sensors[24] or fibre-Bragg gratings.[28,30] Strain gauges have proved to be less sensitive to speed variations than other sensors;[24] moreover, they apply to the evaluation of different quantities that may be bending[14,26] and shear strains.[29] Differently from the majority of past research on travelling load identification, we consider wayside measurements following the approach introduced in Meli and Pugi.[26] Measurements are planned to be carried out where trains run at low speed, which is an advantageous situation in which simplified models describe the response rather well.

In this paper, the inverse problem of load identification is pursued in the time domain, using an estimator that minimizes the difference between the experimental time history of the response, in terms of bending strains, at the foot of the rail and the response provided by the model. The classical Euler–Bernoulli infinite beam resting on a viscoelastic foundation, with the load modelled as a Dirac delta travelling at a constant speed is considered suitable for this inverse problem. It was actually shown[29] that the parametric excitation provided by the discrete supports of the rail and the dynamic effects of the travelling mass can be ignored when far from the critical speed. Moreover, a closed-form solution exists for the related direct problem, making it possible to analytically investigate the response sensitivity to the main mechanical parameters. Models with higher complexity[13,14,26,30,31] may be, instead, more appropriate to describe the direct problem.

Since the train moves at constant speed, position in time and space of loads is clearly determined from the maximum values of the response at the measurement point. Although the actual objective of the procedure is the identification of the train loads, it must be considered that the model contains several parameters, whose values may be more or less uncertain, which have an influence on the load identification. Some authors have dealt with this uncertainty by suggesting an updating of the model parameters using the known load of the locomotor for every train,[24] and others concluded that load identification is viable only in a statistical sense, by defining uncertainty ranges whose amplitude increases with train speed.[29] Another approach to the parameters' uncertainty is by formulating iterative procedures able to simultaneously identify structural parameters and dynamic inputs.[32,33] Here, the load identification problem is formulated in two steps, developing some preliminary work of the authors.[34,35] The first step consists in updating the assumed interpretative model based on the response to a known load. The second step is the actual load identification. Both steps are performed by minimizing the difference between measured and model response quantities, following a traditional approach in load identification[26,29] and in the solution to inverse problems in general.

Solutions to the inverse problem are often ill conditioned in the sense that small changes in the response quantities result in large changes in the calculated load magnitudes. Hence, the procedure is developed within the framework of a Bayesian approach,[36–40] which has the great advantage of analysing the main properties of this inverse problem: identifiability, optimal choice and minimum number of parameters and measurements, as well as problems of well posedness and ill conditioning, not covered by past research. Simulation data, referred to as pseudo-experimental data, are used to quantify the sensitivity of parameter estimation to errors in the known load and the sensitivity of load identification to errors in the model parameters, as well as to investigate the effect of noise on data. Experimental tests were eventually used for validation of the procedure, using a two-axle locomotor whose weight is known from static measurements.

2 | DIRECT PROBLEM

The rail is represented as an Euler–Bernoulli plane infinite beam with constant geometrical and mechanical properties resting on a linear elastic soil with viscous damping and subjected to a Dirac delta load $\delta(z - vt)$ of amplitude P moving at constant speed v. The differential equation of motion is as follows:

$$EI\frac{\partial w^4}{\partial z^4}+\rho A\frac{\partial^2 w}{\partial t^2}+c\frac{\partial w}{\partial t}+kw=P\delta(z-vt), \tag{1}$$

where E is Young's modulus, ρ the density, A the area of the cross section, I its moment of inertia, c the coefficient of viscous damping per unit length, k the soil stiffness per unit length and w the transverse displacement (Figure 1).

The equation of motion (1), with the change of variables $z_1 = z - vt$ and setting $w_1 = w(z_1)$, can be rewritten as an ordinary differential equation in the variable z_1:

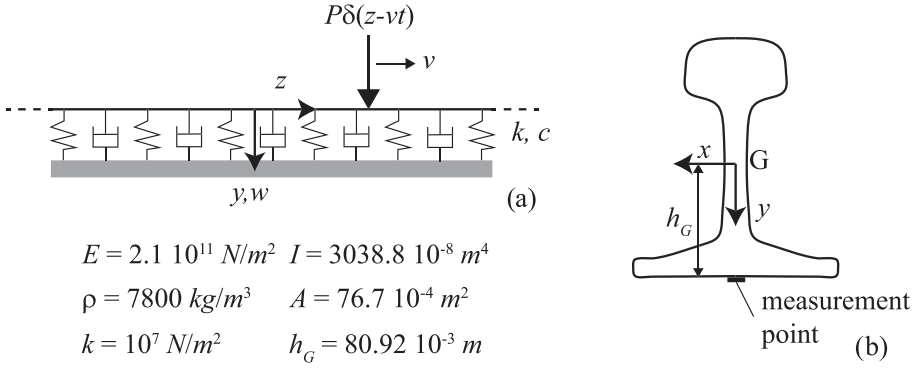

FIGURE 1 Infinite beam resting on a linear viscoelastic soil (a), cross section of the 60 UIC type rail (b) and geometrical and mechanical properties of the system

$$EI\frac{dw_1^4}{dz_1^4}+\rho Av^2\frac{d^2w_1}{dz_1^2}-cv\frac{dw_1}{dz_1}+kw=P\delta(z_1). \tag{2}$$

The complete solution will be of the kind:

$$w_1(z_1)=W_1e^{\kappa_1 z_1}+W_2e^{\kappa_2 z_1}+W_3e^{\kappa_3 z_1}+W_4e^{\kappa_4 z_1} \tag{3}$$

where κ_i, $i=1,..,4$, are the wavenumbers derived from the characteristic equation, with $\kappa_1=\kappa_2^*$, $\kappa_3=\kappa_4^*$ where $(^*)$ stands for complex conjugate. These wavenumbers can represent harmonic travelling waves (κ imaginary), damped waves (κ complex) and evanescent waves (κ real), depending on the train speed and on the geometrical and mechanical parameters of the system. In particular, for $c=0$, $\kappa_i=\pm\sqrt{\left(\rho Av^2\pm\sqrt{(\rho Av^2)^2-4EIk}\right)/EI}$, and we have damped waves with complex κ for $v<v_{cr}=\left(4kEI/(\rho A)^2\right)^{1/4}$, with v_{cr} critical velocity, and propagating waves with imaginary κ for $v>v_{cr}$. The critical velocity is the load speed beyond which undamped waves can freely propagate in time and space. For $c\neq 0$ and $c<c_{cr}=2(k\rho)^{1/2}$ with c_{cr} critical damping, waves are damped irrespective of the train speed. For $c>c_{cr}$, if $v<v_{cr}$ waves are damped, while for $v>v_{cr}$, one couple of waves is damped and one couple is evanescent.

The constants W_1, W_2, W_3 and W_4 have to be determined by enforcing the boundary conditions. First of all, the response has to go to zero at infinity:

$$z_1\to\pm\infty\ w_1=0 \tag{4}$$

$$z_1\to\pm\infty\ \frac{\partial w_1}{\partial z_1}=0; \tag{5}$$

hence, the solution can be separated into its right w_r and left w_l parts, that is,

$$w_r(z_1)=W_1e^{\kappa_1 z_1}+W_2e^{\kappa_2 z_1}\ z_1>0 \tag{6}$$

$$w_l(z_1)=W_3e^{\kappa_3 z_1}+W_4e^{\kappa_4 z_1}\ z_1\leq 0, \tag{7}$$

with $Re(\kappa_1)<0$, $Re(\kappa_2)<0$ and $Re(\kappa_3)>0$, $Re(\kappa_4)>0$. The other boundary conditions to be satisfied are continuity and equilibrium at the point where the load is applied:

$$\left.\frac{dw_l}{dz_1}\right|_{z_1=0}=0;\quad -EI\left.\frac{d^3w_l}{dz_1^3}\right|_{z_1=0}=\frac{P\delta(z_1)}{2} \tag{8}$$

$$\frac{dw_r}{dz_1}|_{z_1=0}=0;\qquad w_l(0)=w_r(0) \tag{9}$$

which finally give

$$w(z,t)=\begin{cases}\dfrac{P}{EI(\kappa_1-\kappa_2)}\left(\dfrac{-e^{(z-vt)\kappa_1}}{(\kappa_1-\kappa_3)(\kappa_1-\kappa_4)}+\dfrac{e^{(z-vt)\kappa_2}}{(\kappa_2-\kappa_3)(\kappa_2-\kappa_4)}\right) & z>0\\ \dfrac{P}{EI(\kappa_3-\kappa_4)}\left(\dfrac{e^{(z-vt)\kappa_3}}{(\kappa_1-\kappa_3)(\kappa_2-\kappa_3)}-\dfrac{e^{(z-vt)\kappa_4}}{(\kappa_1-\kappa_4)(\kappa_2-\kappa_4)}\right) & z\leq 0\end{cases} \tag{10}$$

and, in terms of curvatures:

$$\chi(z,t)=\begin{cases}\dfrac{P}{EI(\kappa_1-\kappa_2)}\left(\dfrac{-\kappa_1^2 e^{(z-vt)\kappa_1}}{(\kappa_1-\kappa_3)(\kappa_1-\kappa_4)}+\dfrac{\kappa_2^2 e^{(z-vt)\kappa_2}}{(\kappa_2-\kappa_3)(\kappa_2-\kappa_4)}\right) & z>0\\ \dfrac{P}{EI(\kappa_3-\kappa_4)}\left(\dfrac{\kappa_3^2 e^{(z-vt)\kappa_3}}{(\kappa_1-\kappa_3)(\kappa_2-\kappa_3)}-\dfrac{\kappa_4^2 e^{(z-vt)\kappa_4}}{(\kappa_1-\kappa_4)(\kappa_2-\kappa_4)}\right) & z\le 0.\end{cases} \tag{11}$$

In the following examples, we will assume that the beam has the mechanical and geometric characteristics of a 60 UIC type rail (see Figure 1, which shows also its cross section), with h_G vertical distance between the centre of mass and the foot of the rail. According to the research work in Lei,[4] when calculating the distributed mass of the beam, the mass of the sleepers and part of the mass of the ballast should be added to the mass of the rail, leading to a collaborating mass of 2700 kg/m. In our case, this results in a critical velocity $v_{cr}=277$ km/h, which can only be reached by high-speed trains.

The time history of the response in terms of microstrains at the foot of the rail $\mu\epsilon$ at $z=0$ for $P=1$ N is represented in Figure 2, for different speeds and damping. These strains correspond to the response quantity measured in the experimental tests and are tied to the curvature of Equation (11) by the linear relation $\epsilon=h_G\chi$ (Figure 1b), valid for small displacements. Figure 2a shows that for speeds of 28 km/h approximately corresponding to $0.1v_{cr}$, the dependence of the maximum amplitude on damping is very limited. When the speed increases, the response is no longer symmetric (Figure 2b), and the maximum amplitude depends increasingly on the train speed (Figure 2a–c). For a speed equal to the critical velocity, a resonance occurs: the maximum response increases and, as expected, depends greatly on damping (Figure 2c). As the speed increases, higher frequencies are involved, as it emerges from the Fourier transform reported

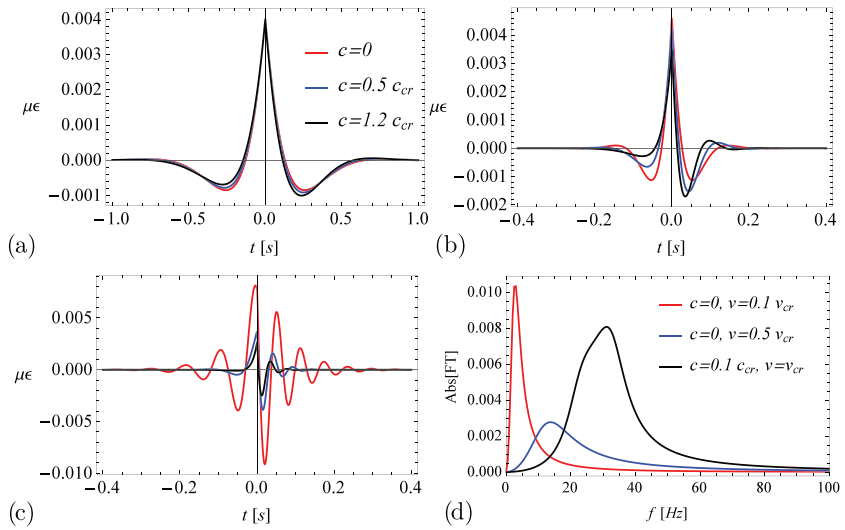

FIGURE 2 Time histories of strains for different values of damping and speed: 28 km/h=$0.1v_{cr}$ (a), 140 km/h = $0.5v_{cr}$ (b), 280 km/h = v_{cr} (c) and absolute value of the Fourier transform of three time histories of strains for increasing speed (d)

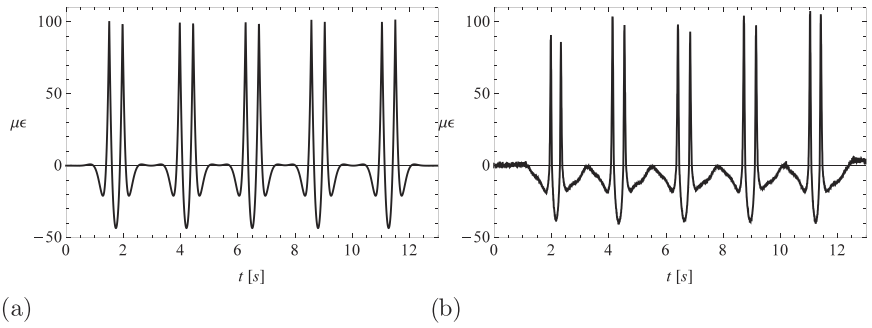

FIGURE 3 Analytical (a) and experimental (b) strain time histories of an ETR324

in Figure 2d for three strain time histories with increasing speed and no damping (except the case of $v = v_{cr}$ when $c = 0.1c_{cr}$ was assumed to avoid unbounded response). It is apparent that the maximum frequency involved, defined as the frequency whose Fourier transform amplitude is 20% of the maximum value, increases from 10 ($v = 0.1v_{cr}$) to 40 ($v = 0.5v_{cr}$) and finally to 50 Hz ($v = v_{cr}$). This has consequences for the minimum sampling frequency required for experimental recordings.

Figure 3a shows the analytical time history of the strains caused by a series of 10 Dirac delta loads with $P = 78{,}400$ N, which is approximately the load acting on one wheel of an unladen ETR324, obtained using Equation (1) with a travelling speed of 22 km/h. Figure 3b reports, for comparison, the same quantity, experimentally measured, for an ETR324, travelling at around the same speed. The pattern of the time history obtained from the model satisfactorily agrees with the time history observed experimentally, which guarantees that the model is potentially fit to represent experimental observations.

3 | INVERSE PROBLEM

The goal of the solution of the inverse problem consists in the identification of the amplitudes of the Dirac deltas representing train loads. Actually, trains are composed of a number of carriages, and $\mathbf{P}$ is an l-element vector, whose components P_i represent the load carried by each wheel. This situation can be modelled by linear superposition of strains caused by unit loads ϵ_1 with a delay $\tau_i = d_i/v$, where d_i is the spacing between the first and the ith axles:

$$\epsilon(t) = \sum_{i}^{l} P_i \epsilon_1(t - \tau_i). \tag{12}$$

In the sensitivity analysis developed using pseudo-experimental data, one single load P will be considered. The train speed v is directly measurable and will not be one of the unknowns of the problem. The model contains several parameters, whose values may be more or less uncertain, that have an influence on the result of the load identification, which is the actual goal of the procedure. These parameters are the object of a preliminary model updating, made on the basis of the response to a known load. The mechanical and geometrical parameters that govern the model response are ρA, EI, k and c. Damping is a parameter on whose value there is little agreement in scientific literature.[24] Since the measurements can be performed for trains running at low speed, in view of the results obtained with the direct problem, it was assumed $c = 0$. The vector of unknown model parameters will then be $\{\rho A, EI, k\}^T$.

Let us call $\epsilon(\mathbf{x})$ the vector of observed quantities as a function of $\mathbf{x}$, which is an n-element vector that can be either the vector of model parameters in a problem of parameter estimation or the load vector for load identification. Let $\mathbf{z}$ be the m-element vector of measured quantities, that is, the experimental response sampled in time. One measurement at a single location will provide sufficient information to solve the inverse problem, although the procedure could be easily applied to more than one measurement point by adding the data to the vector $\mathbf{z}$. A higher amount of measurement locations can be beneficial in the presence of experimental errors but are not strictly necessary. The vector of observed quantities is an m-element vector $\epsilon(\mathbf{x}) = \{\epsilon_1(\mathbf{x}), \ldots \epsilon_m(\mathbf{x})\}^T$, whose ith element represents the strain sample provided by the model at a given abscissa and at the ith time instant. The vector $\epsilon(\mathbf{x})$ is related to the vector of measured quantities $\mathbf{z}$ by the following equation:

$$\mathbf{z} = \epsilon(\mathbf{x}) + \mathbf{n} \tag{13}$$

where $\mathbf{n}$ is assumed to be a zero-mean white-noise vector, independent of $\mathbf{x}$. Unknowns $\mathbf{x}$ can be considered random variables that benefit from the a priori information of a Bayesian approach. According to this approach, the best estimate $\hat{\mathbf{x}}$ is the vector that maximizes the occurrence of $\mathbf{x}$, given the measured quantities $\mathbf{z}$. The function $p(\mathbf{x}|\mathbf{z})$ is the a posteriori probability density of the parameters $\mathbf{x}$ obtained given the measurements $\mathbf{z}$.[36,39] Assuming a normal distribution for $\mathbf{x}$ and $\mathbf{n}$, and $\mathbf{S_x}$ ($n \times n$) and $\mathbf{S_n}$ ($m \times m$) being the positive definite covariance matrices of the unknowns and of the noise, respectively, the maximum of the probability $p(\mathbf{x}|\mathbf{z})$ is attained for a value $\hat{\mathbf{x}}$, which minimizes the objective function:

$$l(\mathbf{x}) = [\mathbf{z} - \boldsymbol{\epsilon}(\mathbf{x})]^T \mathbf{S}_\mathbf{n}^{-1} [\mathbf{z} - \boldsymbol{\epsilon}(\mathbf{x})] + (\mathbf{x} - \mathbf{x}_0)^T \mathbf{S}_\mathbf{x}^{-1} (\mathbf{x} - \mathbf{x}_0). \tag{14}$$

The first term of $l(\mathbf{x})$ takes into account the difference between measured and model-predicted quantities, while the second considers the distance between $\mathbf{x}$ and the initial estimate $\mathbf{x}_0$, both weighted by the inverse of the covariance matrices of noise and parameters, respectively. In general, the response quantities depend nonlinearly on the model parameters, while their dependence on the load $\mathbf{P}$ is linear, as it is obvious from Equation (11).

Local identification is assured when the conditions that (i) the first derivative of $l(\mathbf{x})$ with respect to unknowns is null and (ii) its Hessian matrix $\mathscr{H}$ is positive definite are satisfied in a connected subspace of the unknowns space. Within this context, linearizing the objective function in the neighbourhood of $\mathbf{x}_0$, its minimum is for

$$\hat{\mathbf{x}} = \mathbf{x}_0 + (\mathbf{H}^T \mathbf{S}_\mathbf{n}^{-1} \mathbf{H} + \mathbf{S}_\mathbf{x}^{-1})^{-1} \mathbf{H}^T \mathbf{S}_\mathbf{n}^{-1} (\mathbf{z} - \boldsymbol{\epsilon}(\mathbf{x}_0)), \tag{15}$$

where $\mathbf{H}$ is an $(m \times n)$ sensitivity matrix with components $H_{ij} = \partial \epsilon_i / \partial x_j$ and $\mathbf{S} = (\mathbf{H}^T \mathbf{S}_\mathbf{n}^{-1} \mathbf{H} + \mathbf{S}_\mathbf{x}^{-1})^{-1}$ is the a posteriori covariance matrix. Within this linearized framework, the Hessian matrix writes $\mathscr{H} = \mathbf{H}^T \mathbf{S}_\mathbf{n}^{-1} \mathbf{H} + \mathbf{S}_\mathbf{x}^{-1}$ whose first term $\mathbf{A} = \mathbf{H}^T \mathbf{S}_\mathbf{n}^{-1} \mathbf{H}$ is called Fisher or information matrix. When the relationship between unknowns and measured quantities is nonlinear, as in the case of parameter estimation, Equation (15) is applied iteratively, providing a better estimate at each iteration. When the relationship is linear, as in the case of load identification, Equation (15) directly provides the best estimate; in fact, the matrix $\mathbf{A}^{-1}$ corresponds to the weighted pseudo-inverse.

The characteristics of the inverse problem will be investigated using the response of the system in Figure 1 in terms of strains at the foot of the rail, for a single unit load P, travelling at a speed $v = 0.1 v_{cr}$ km/h. The same system will be used to generate the pseudo-experimental data used in Section 3.1. Figure 4a reports the time history of the percentage change of the strain for a 10% variation of each of the three parameters ρA, EI and k. The percentage is calculated in relation to the maximum value of the strain that occurs at the time $t = 0$ s. These time histories are proportional to the columns of the $m \times 3$ sensitivity matrix. Figure 4a shows that, among the mechanical parameters, EI and k are the most important, while ρA has little influence, as can be expected by the quasi-static character of the response for low train speed.

Identifiability is the actual possibility to determine a single set of optimal parameters $\hat{\mathbf{x}}$ so that the objective function is at a minimum. Here, convexity of the objective function is guaranteed locally by the positive definiteness of $\mathscr{H}$, due to its structure and the positive definiteness of covariance matrices. Some information about identifiability is provided by $\mathbf{H}$, whose rank indicates the maximum number of identifiable parameters: in the present case, the rank of $\mathbf{H}$ is 3, taking at least the minimum number of samples nonsymmetric with respect to the response peak ($m = 3$). On the contrary, if symmetric samples are taken, three samples are not sufficient, and at least five of them are necessary for $\mathbf{H}$ to have rank 3, meaning that symmetric data do not add independent information. For load identification, in the absence of noise, a single sample per unknown load is theoretically sufficient.

More precise information on the choice of parameters and measurements is provided by the Fisher matrix, which must be invertible for the solution to (15) to be calculated. It should be noted that the rank of the Fisher matrix equals the rank of $\mathbf{H}$. The list of the eigenvalues of $\mathbf{A}$ can put the parameters, or more frequently, their linear combination, in order of importance. This is displayed by the shape of the eigenvectors, which enables the possible coupling between

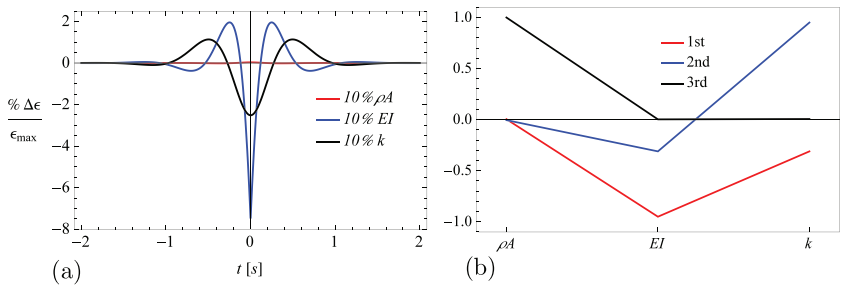

FIGURE 4 Time histories of the per cent change of base strain for a 10% variation of mechanical parameters (a) and the eigenvectors of the Fisher matrix with the maximum value set to 1 (b)

parameters to be recognized. The eigenvectors of the rank-three 3×3 Fisher matrix, whose rows and columns correspond to the parameters ρA, EI and k are reported in Figure 4b. They enable one to conclude that the parameters EI and k are coupled, while ρA is an independent parameter with little influence on the response. In fact, the related eigenvector has only the first component different from zero and is associated with the smallest eigenvalue, which is nearly 13 orders of magnitude smaller than the first two. In such situation, it seems to be appropriate to discard the parameter ρA and estimate the optimal EI and k only, using the response to a known load, with a 2×2 $\mathbf{A}$ matrix.

The flowchart in Figure 5 summarizes the procedure described in this section, which entails a preliminary model updating using the response to a known load, followed by the actual load identification, depicted in Figure 5 for the general case of more than one load.

3.1 | Pseudo-experimental data

The procedure proposed is first applied to pseudo-experimental data to investigate the main features of the inverse problem and then, in the following subsection, is applied to experimental data.

Here, using a pseudo-experimental time history of strains generated by a unit known load, in the absence of noise, we proceed to identify two parameters, EI and k. Given that the analysis is performed in the absence of noise, it is assumed that $\mathbf{S_n}$ is an identity matrix and $\mathbf{S_x^{-1}}$ is null, so that no restriction is posed on parameter variation. Three different couples of samples, as shown in Figure 6a, are taken as pseudo-experimental data. In particular, two nonsymmetric samples close to the points of maximum sensitivity (b, red points), two nonsymmetric samples distant from the maximum sensitivity (c, black) and two symmetric samples (d, green) are considered. Figure 6b–d reports the objective functions of Cases B, C and D, respectively. In all the contour plots, the objective function is made non-dimensional by dividing its value by the maximum square value of the response and by the number of samples m. The labels on the contour lines indicate the related value. On comparing Figure 6b and Figure 6c, it can be seen that in both cases, the objective function is smooth and has a unique minimum, but when samples are taken close to the points of maximum sensitivity (B), the objective function is more convex. In Case C, much of the curvature in direction EI is lost. In both Cases B and C, even starting from initial parameters with a 20% error, convergence to the exact values occurs within three and four iterative applications of Equation (15), respectively. Using the identified parameters, and proceeding to the identification of the load, its exact value is evaluated with one single application of Equation (15). On choosing symmetric points (Case D), the objective function has multiple minima placed along the black line of Figure 6d. In this case, the 2×2 Fisher matrix has rank 1; therefore, EI and k are not uniquely identifiable, since the two symmetric samples are not independent data. It can be concluded that at least two samples nonsymmetric with respect to the maximum are necessary and sufficient to identify EI and k.

Inverse problems are often difficult because they are ill conditioned. Therefore, it is of interest to investigate the sensitivity of parameter estimation to errors in the known load, as well as the sensitivity of load identification to errors in the model parameters. In the first step of parameter estimation, the response to a known load has to be available. In practice, the load is due to a vehicle in motion, which can be statically weighted but, when it travels along the track, can give rise to an uneven distribution of the weight on the wheels, due to vehicle imbalance and irregularities of the

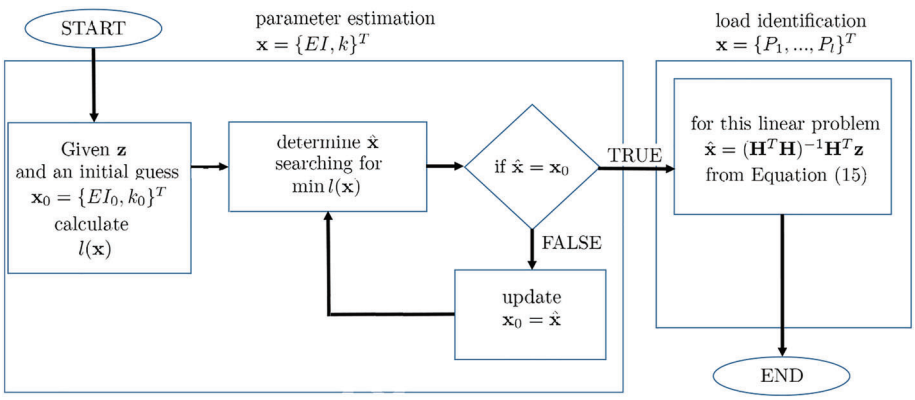

FIGURE 5 Flowchart of the load identification procedure

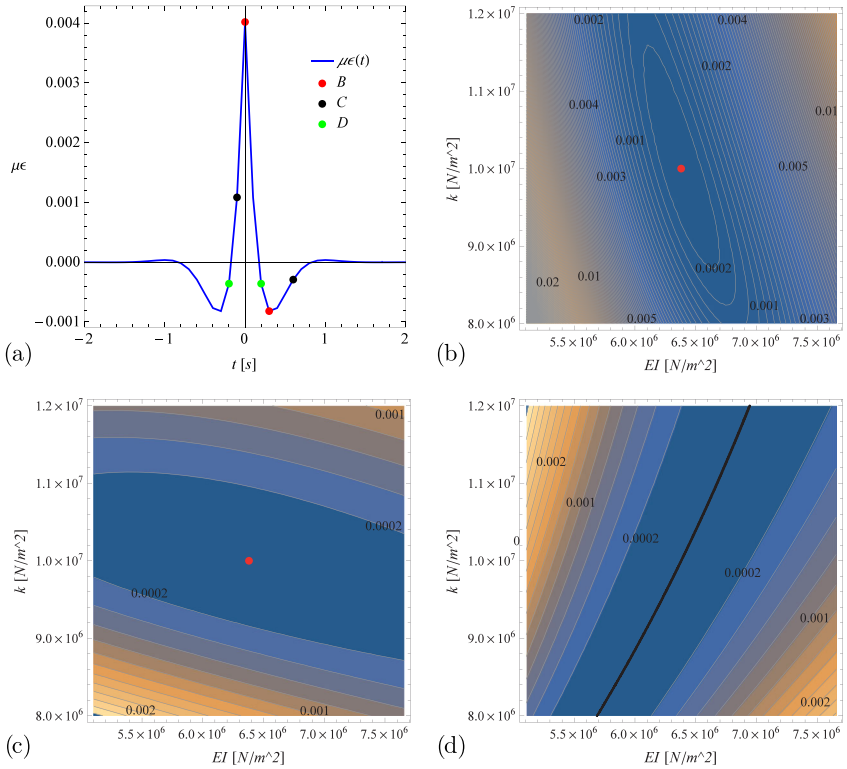

FIGURE 6 Strain samples of pseudo-experimental data in the absence of noise and (a) contour plots of the related objective function for the (b) red samples, (c) black samples and (d) green samples

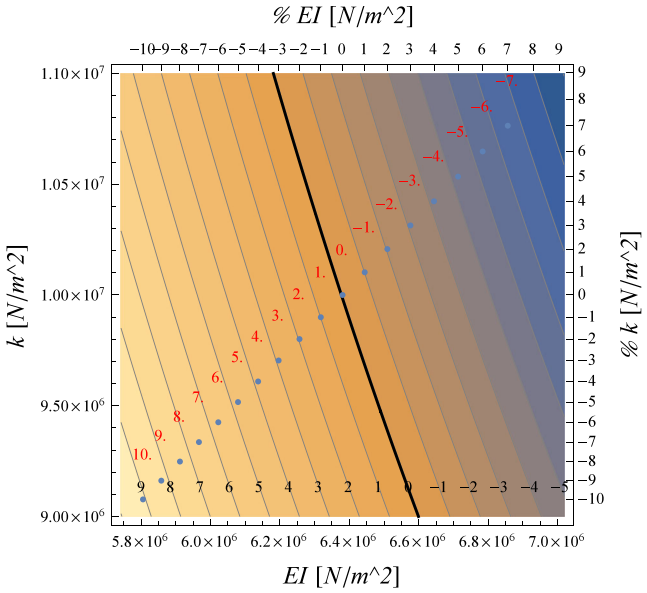

FIGURE 7 Per cent errors on the identified load due to errors in the parameters (contours, black labels) and per cent errors in parameter estimate due to errors in the known load (blue points, red labels)

track supports. The weight in motion can therefore differ from its static counterpart, resulting in an error on the estimated *EI* and *k* that varies as shown in Figure 7 (upper and right frame labels for errors in percentage). The coordinates of each blue point are the estimated values of *EI* and *k* when the known load embodies an error as defined in per cent by the red labels. It should be noticed that an underestimation of the load results in an overestimation of the stiffness parameters, and vice versa. Moreover, the error on the estimates of *EI* and *k* is locally almost linear: an underestimation

of the load of −7% (upper right blue point, red label) gives an overestimation of EI and k of around the same amount. In turn, an error in the estimate of the system parameters affects load identification. The related sensitivity is presented again in Figure 7 by means of a contour plot of the error on the identified load (black labels) as a function of the model parameters EI and k. This figure shows that there are couples of values EI and k belonging locally to straight lines to which the same error on the identified load corresponds. The thick black line corresponds to a nearly null error on the load.

Another important point is the effect of noise, which was investigated by adding to the pseudo-experimental time-history a zero-mean Gaussian white noise vector $\mathbf{n}$ (Equation 13), which makes it possible to evaluate the goodness of the estimator and perform a posteriori estimates of the variance of the identified quantities and of the error on their mean value. The noise had large standard deviation, equal to 20% of the root-mean-square value of the strain in the time range $-2s$, $2s$. The covariance matrix of the noise $\mathbf{S_n}$ was taken as an identity matrix: in this way, all the samples are equally weighted, with the result that those with a greater value will have a greater importance. Also in this case, the inverse of the covariance matrix of parameters $\mathbf{S_x^{-1}}$ was assumed null, which means that the domain of parameter search is not restricted. Three time history realizations of strains used as input data are reported in Figure 8a,c,e, with decreasing time steps $dt = 0.05, 0.01, 0.001$ s, corresponding to, respectively, 41, 201 and 2001 strain samples and to sampling frequencies of 20, 100 and 1000 Hz. The minimum sampling frequency used is 20 Hz, which can describe strain

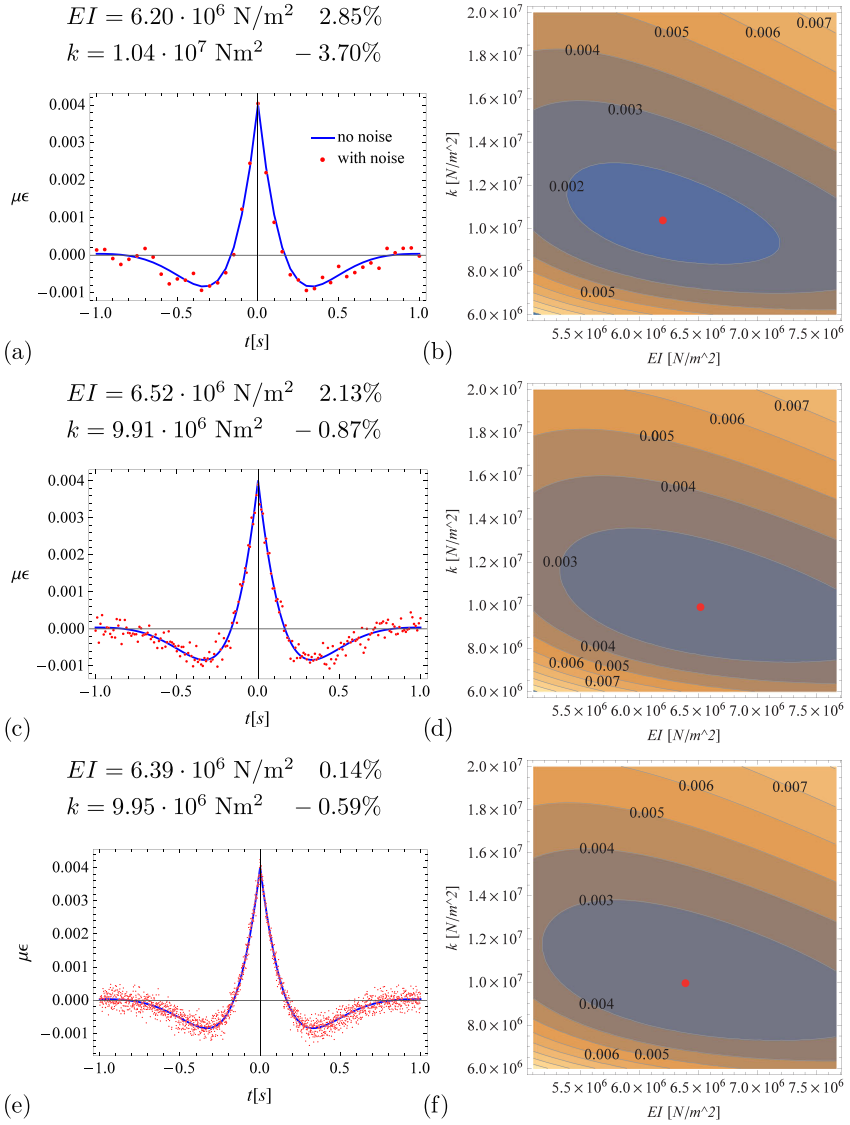

FIGURE 8 Time histories of strains with increasing number of samples and related objective functions and identified parameters with per cent error (a, b) $m = 41$, (c, d) $m = 201$ and (d, e) $m = 2001$

time histories with a maximum frequency content of 10 Hz, in compliance with the Nyquist theorem (see Figure 2d). When comparing responses at different speeds, the sampling frequency has to be altered accordingly. Figure 8b,d,f also reports the corresponding contour plots of the objective functions, showing that they are smooth and have a single minimum. The values of the identified *EI* and *k* together with their errors are also listed in Figure 8: by increasing the number of samples, the error remarkably reduces. This is better shown in Figure 9, where the red points represent the estimated *EI* and *k* obtained from a total of 30 different realizations with 41 (a), 201 (b) and 2001 (c) samples, superimposed on the contour plot of the error committed on the load of Figure 7. It can be noticed that when a low number of samples is used (Figure 9a), the identified values are too spread out. By increasing the number of samples (Figure 9b,c), the identified parameters form a narrow cloud of points in the neighbourhood of the correct values, with a limited error on the identified load. A quantitative measure of this result is given in Table 1, which reports, for each of the three cases, the error on the mean value e_μ and the related coefficient of variation c_v (ratio between standard deviation and expected value), both in per cent values. The error e_μ is very limited and smaller than 1%. The coefficient of variation of the estimates is very limited as well and smaller than that of the noise in data. In the cases with 2001 and 201 samples, the error on the load will be respectively in the range ±1% and ±3%, which is quite satisfactory. In general, high-frequency experimental recordings are available; therefore, such precision on the identified parameters is theoretically in reach. However, other sources of error may be present and can affect the estimates. In the experimental

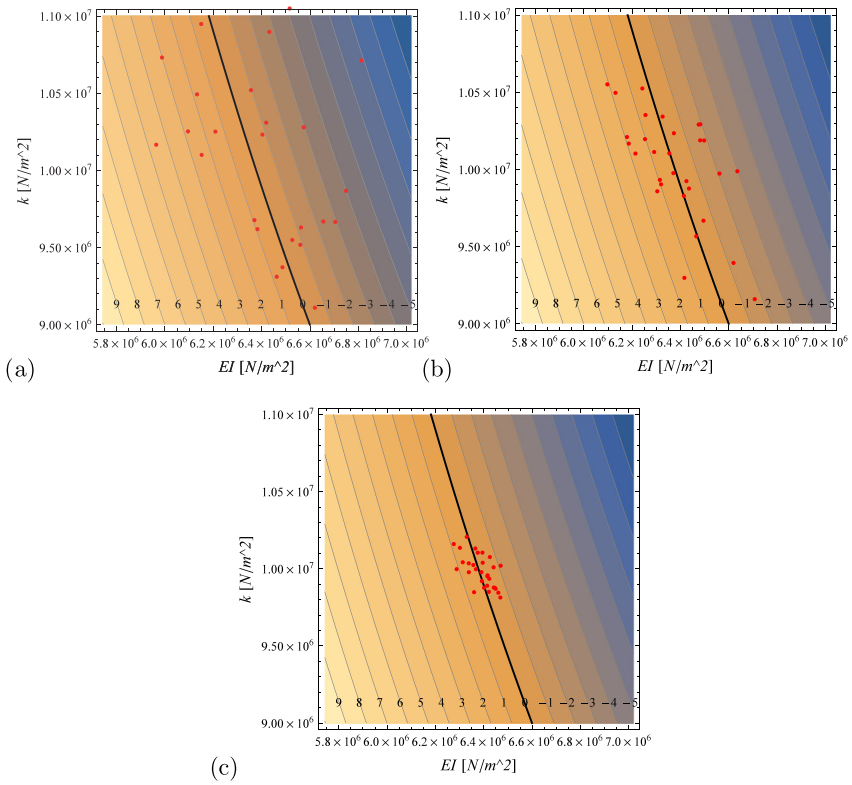

FIGURE 9 Identified values (points) of *EI* and *k* obtained from cases with $m = 41$ (a), 201 (b) and 2001 (c) samples and related error expected on the identified load (contours)

TABLE 1 Error on the mean value e_μ and coefficient of variation c_v in per cent values obtained for cases with $m = 41$ (a), 201 (b) and 2001 (c) samples

	(a)		(b)		(c)	
	e_μ	c_v	e_μ	c_v	e_μ	c_v
EI	0.20	4.2	0.15	2.3	0.13	0.8
k	0.56	8.1	0.24	3.8	0.15	1.2

tests, a sampling frequency f_s of 100 Hz is adopted for a speed of around 25 km/h and then adjusted maintaining approximately the same ratio f_s/v.

3.2 | Experimental data

In this subsection, identification is performed using wayside experimental strains recorded by a resistive strain gauge at the foot of a rail placed on an embankment, passed over by a locomotor moving at low speeds. The sensors TML FLAB-6-11 foil strain gauges, with a resistance of 120 Ω and maximum strain 5%, were installed. The gauge has a frequency response limit of around 250 kHz. A total of five transits of the locomotor are available, with increasing constant speeds (Table 2) and maximum speed around 1/10 of the critical velocity. A picture and a sketch of the locomotor, whose total weight is known from static measurements and assumed to be equally distributed on the wheels, are reported in Figure 10a,b, respectively. A sampling frequency of 1000 Hz was used in the experimental recordings, which is quite high based on the results of the previous subsection. The experimental signals were therefore downsampled adjusting the sampling frequency to the different speeds, as reported in Table 2. The rail strain is affected by temperature, but this effect can be omitted because the variations of strains due to the train transit take place in a short space of time. In this experimental application, the inverse of covariance matrices of parameters $\mathbf{S}_\mathbf{x}^{-1}$ was assumed null. This is because the parameters are difficult to be reliably estimated a priori.[14,29,33] As concerns the parameter EI, although Young's modulus of the material and the cross section of the rail are known, the possibility that the sleepers and ballast also provide an additional contribution to the bending stiffness was thus taken into account. The covariance of the noise $\mathbf{S_n}$ was taken as an identity matrix, to equally weigh all the absolute differences between measured data and model response.

The time histories of the slowest and the fastest transits (1 and 5) were used to identify the flexural stiffness EI and the soil stiffness k, in order to embed possible effects tied to the speed change. The identified values of these parameters are reported in Figure 11 together with the objective functions and the related experimental and optimized-model time histories. In the updated model, the mean values $EI = 6.98 \cdot 10^6$ and $k = 4.45 \cdot 10^7$ N/m^2 were used. The estimated EI is quite close to the value $6.38 \cdot 10^6$ N/m^2 obtained from the geometry of the rail and the reference value of E reported in Figure 1. It can be observed that the objective functions obtained with experimental data maintain a remarkable resemblance to those of the pseudo-experimental case (Figure 7), exhibiting smoothness and a single minimum, although the experimental objective function is less convex and, of course, never reaches a null value.

TABLE 2 Identified loads and errors on the single loads and on the total load

transit	v (km/h)	f_s (Hz)	P_1 (kN)	% err$_1$	P_2 (kN)	% err$_2$	% err$_T$
1	5.22	20	39.11	1.4	39.11	1.4	1.4
2	7.85	50	36.77	−4.6	38.30	−0.7	−2.7
3	12.46	50	39.84	3.3	40.54	5.1	4.2
4	19.51	100	36.90	−4.3	40.26	4.4	0.1
5	24.01	100	35.98	−6.7	40.27	4.5	−1.1

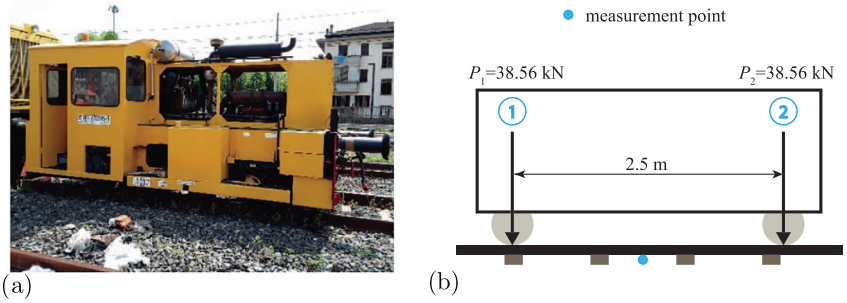

FIGURE 10 Picture (a) and sketch (b) of the locomotor

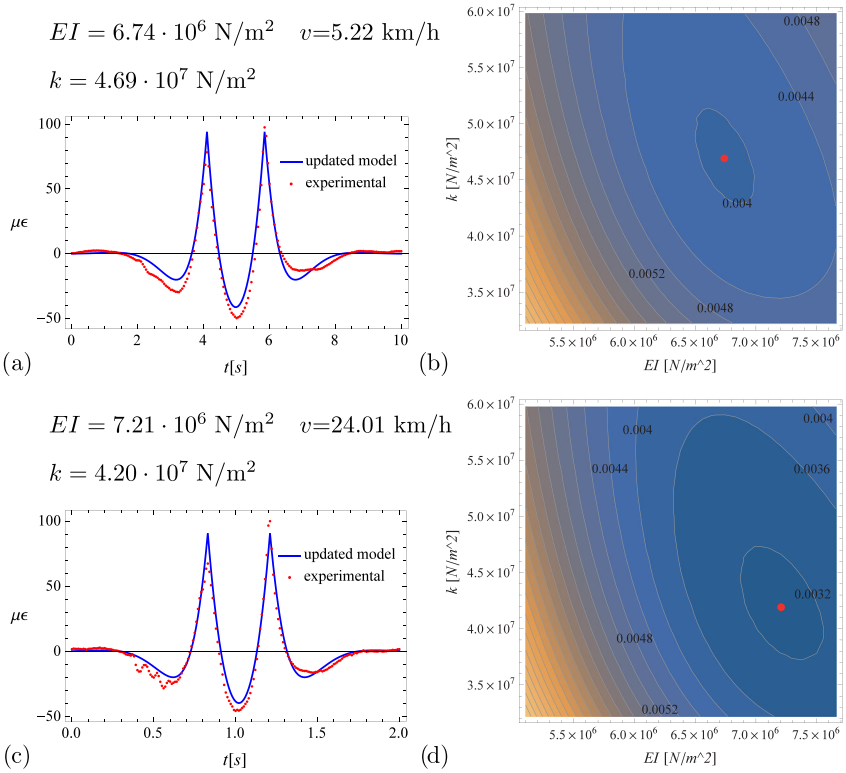

FIGURE 11 Experimental and updated-model time histories at different speeds (a, c) and the related objective functions (b, d)

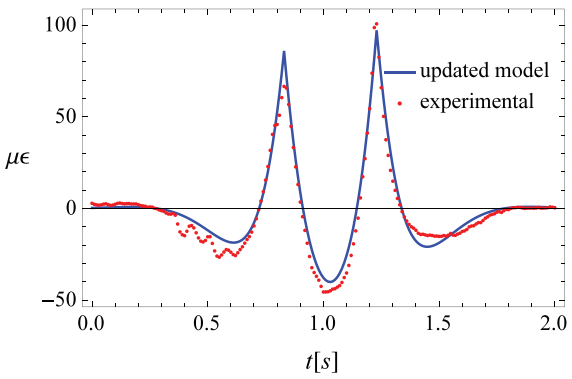

FIGURE 12 Experimental and updated model with identified load time histories of the fourth transit

In the end, the updated model was used to identify the travelling locomotor loads that are considered, at this point, as unknowns. It should be noted that in this experimental case, the unknown load is a two-component vector $\mathbf{P} = \{P_1, P_2\}$ (Figure 10c). The identified loads and the related errors are reported in Table 2, together with the error on the total load err_T. Table 2 shows that the identified load values are in close agreement with the expected ones, with errors not greater than 5% on the total weight of the locomotor and mean absolute error smaller than 2%. The error obtained is comparable with that obtained by other authors using more complex models[19,26,29] and could be further reduced with an experimental setup measuring strains on the two rails and using their mean.[26] As obtained in Mosleh et al,[29] the error on the total load $\mathbf{P}$ is smaller than the error on its components P_1 and P_2 because the effects of imbalance are compensated. Figure 12 shows a comparison between the experimental time histories of strains of a transit and those obtained from the updated model with the identified loads, demonstrating a close agreement between experimental data and response of the updated model, with a mean difference of the 4% of the maximum experimental response.

4 | CONCLUSIONS

This paper has presented an approach to the identification of travelling loads of trains based on the minimization of the difference between the experimental time history of strains at the base of the rail and its analytical counterpart. The model describing the response was a one-dimensional plane infinite Euler–Bernoulli beam resting on a viscoelastic soil. The loads were modelled as Dirac deltas travelling at constant speed. Damping was proved to not be significant for an appropriate description of the response in the range of speeds far from the critical value, which is appropriate to deal with this problem. Within a Bayesian approach, a sensitivity analysis, based also on the investigation of eigenvalues and eigenvectors of the Fisher matrix, produces the result that, among the model parameters, the soil and the beam stiffness are two coupled independent parameters, with the most relevant influence on the response, while the mass density turned out to be an independent parameter with negligible effect for low train speed.

The identification of the travelling loads was performed in two steps: first, estimating the optimal model parameters EI and k using the response to a known load and then using the updated model to actually identify the train loads. The characteristics of the inverse problem were investigated using pseudo-experimental data in the absence and presence of noise. As regards the minimum number of response samples, it was shown that, in the absence of errors, two strain samples that are nonsymmetric with respect to the time instants of maximum response are necessary and sufficient to the model updating, better if close to the points of maximum sensitivity, which guarantees greater convexity of the objective function. The sensitivity of the results of parameter estimation to errors in the known load and the sensitivity of load identification to errors in the model parameters were investigated. It was shown that errors on the model parameters in the range $\pm 10\%$ cause an error on the identified load of similar magnitude. Furthermore, an analysis performed on noisy data showed that, in the presence of errors, a much higher amount of data are necessary than those necessary and sufficient if limited error on the identified load is sought. In particular, the sampling frequency f_s has to be adapted to the train velocity, and a ratio $f_s/v > 4$ Hz/(km/h) should be used.

Experimental field tests were also performed, in which the strains at the foot of the rail caused by five transits of a known-weight locomotor at low speed were recorded. With reference to the slowest and fastest transits, the model was updated by identifying the optimal values of rail and soil stiffness and, afterwards, used as an interpretative model to identify the weight of the locomotor in all the transits. The loads, assumed as unknowns, were identified with satisfactory accuracy, with a mean absolute error on the total load smaller than 2%, proving the appropriateness of the simple model employed in this inverse problem for speeds not exceeding 10% of the critical speed. The experimental time histories and those of the updated model with identified loads were shown to be in close agreement.

ACKNOWLEDGEMENTS

The authors would like to gratefully acknowledge the partial funding of the research on behalf of the company Ace System and the joint cooperation in performing the experimental measurements with Giuliano Manganozzi, from the DISG Laboratory, Sapienza University of Rome. The partial support of EU (grant agreement number RFCS-2018_800687) and of Sapienza Research Grants 2018 RP1181642D8B9FAF and 2020 RM120172B397172A is also gratefully acknowledged.

AUTHOR CONTRIBUTION

Annamaria Pau: conceptualization (equal); methodology (equal); investigation (equal); writing - original draft (lead); writing - review and editing (lead); software (lead). Fabrizio Vestroni: conceptualization (equal); methodology (equal); investigation (equal); writing - review and editing (supporting).

DATA AVAILABILITY STATEMENT

Data subject to third party restrictions

ORCID

Annamaria Pau https://orcid.org/0000-0002-4946-0302
Fabrizio Vestroni https://orcid.org/0000-0001-9299-0678

REFERENCES

1. Timoshenko SP. Methods of analysis of statistical and dynamical stresses in rails, *Proceedings of the 2nd International Conference of Applied Mechanics*, Zürich, Switzerland; 1927:1–12.

2. Kenney JT. Steady-state vibration of beam on elastic foundation for moving load. *J Appl Mech-T ASME*. 1954;76:359-364.
3. Fryba L. *Vibrations of Solids and Structures under Moving Loads*. Groningen: Noordhoff International Publishing; 1972.
4. Lei X. Analytic method for dynamic analysis of the track structure. In: *High Speed Railway Track Dynamics*. Springer; 2017:37-56.
5. Chen Y-H, Huang Y-H. Dynamic stiffness of infinite Timoshenko beam on viscoelastic foundation in moving co-ordinate. *Int J Numer Methods Eng*. 2000;48(1):1-18.
6. Murray CA, Take WA, Hoult NA. Measurement of vertical and longitudinal rail displacements using digital image correlation. *Can Geotech J*. 2015;52(2):141-155.
7. Milne D, Pen LL, Thompson D, Powrie W. Automated processing of railway track deflection signals obtained from velocity and acceleration measurements. *P I Mech Eng F-J Rai*. 2018;232(8):2097-2110.
8. Wheeler LN, Take WA, Hoult NA, Le H. The use of fiber optic sensing to measure distributed rail strains and determine rail seat forces due to a moving train. *Can Geotech J*. 2019;56(1):1-13.
9. Mallik AK, Chandra S, Singh AB. Steady-state response of an elastically supported infinite beam to a moving load. *J Sound Vib*. 2006; 291(3-5):1148-1169.
10. Miao Y, Shi Y, Wang G, Zhong Y. Closed-form solution of beam on Pasternak foundation under inclined dynamic load. *Acta Mech Solida Sin*. 2017;30(6):596-607.
11. Castro Jorge P, Simoes FMF, Pinto da Costa A. Dynamics of beams on non-uniform nonlinear foundations subjected to moving loads. *Comput Struct*. 2015;148:26-34.
12. Shamalta M, Metrikhine AV. Analytical study of the dynamic response of an embedded railway track to a moving load. *Arch Appl Mech*. 2003;73:131-146.
13. Hall L. Simulations and analyses of train-induced ground vibrations in finite element models. *Soil Dyn Earthq Eng*. 2003;23(5):403-441.
14. D'Adamio P, Marini L, Meli E, Pugi L, Rindi A. Development of a dynamical weigh in motion system for railway applications. *Meccanica*. 2016;51(10):2509-2533.
15. Ying Z-G, Ni Y-Q, Kang L. Mode localization characteristics of damaged quasiperiodically supported beam structures with local weak coupling. *Struct Control Health*. 2019;26(6):e2351.
16. Sun YQ, Dhanasekar M. A dynamic model for the vertical interaction of the rail track and wagon system. *Int J Solids Struct*. 2002;39(5): 1337-1359.
17. Law S-S, Zhu X-Q. *Moving Loads—Dynamic Analysis and Identification Techniques*. London: Taylor and Francis Group; 2011.
18. Ouyang H. Moving-load dynamic problems: a tutorial (with a brief overview). *Mech Syst Signal Proc*. 2011;25(6):2039-2060.
19. Yu Y, Cai CS, Deng L. State-of-the-art review on bridge weigh-in-motion technology. *Adv Struct Eng*. 2016;19(9):1514-1530.
20. Trujillo DM, Busby HR. *Practical Inverse Analysis in Engineering*. CRC press; 1997.
21. Chan THT, Yu L, Law SS. Comparative studies on moving force identification from bridge strains in laboratory. *J Sound Vib*. 2000;235 (1):87-104.
22. Johansson A, Nielsen JCO. Out-of-round railway wheels: wheel-rail contact forces and track response derived from field tests and numerical simulations. *P I Mech Eng F-J Rai*. 2003;217(2):135-146.
23. Ronasi H, Johansson H, Larsson F. A numerical framework for load identification and regularization with application to rolling disc problem. *Comput Struct*. 2010;89:38-47.
24. Sekuła K, Kołakowski P. Piezo-based weigh-in-motion system for the railway transport. *Struct Control Health*. 2012;19(2):199-215.
25. Milković D, Simić G, Jakovljević Z, Tanasković J, Lučanin V. Wayside system for wheel–rail contact forces measurements. *Measurement*. 2013;46(9):3308-3318.
26. Meli E, Pugi L. Preliminary development, simulation and validation of a weigh in motion system for railway vehicles. *Meccanica*. 2013; 48(10):2541-2565.
27. Roveri N, Carcaterra A, Sestieri A. Real-time monitoring of railway infrastructures using fibre Bragg grating sensors. *Mech Syst Signal Proc*. 2015;60:14-28.
28. Kouroussis G, Kinet D, Moeyaert V, Dupuy J, Caucheteur C. Railway structure monitoring solutions using fibre Bragg grating sensors. *Int J Rail Transp*. 2016;1-16.
29. Mosleh A, Alves Costa P, Calçada R. A new strategy to estimate static loads for the dynamic weighing in motion of railway vehicles. *P I Mech Eng F-J Rai*. 2020;234(2):183-200.
30. Liu X-Z, Xu C, Ni Y-Q. Wayside detection of wheel minor defects in high-speed trains by a Bayesian blind source separation method. *Sensors*. 2019;19(18):3981.
31. Koh CG, Ong JSY, Chua DKH, Feng J. Moving element method for train-track dynamics. *Int J Numer Methods Eng*. 2003;56(11): 1549-1567.
32. Sun H, Betti R. Simultaneous identification of structural parameters and dynamic input with incomplete output-only measurements. *Struct Control Health*. 2014;21(6):868-889.
33. Feng D, Sun H, Feng M. Simultaneous identification of bridge structural parameters and vehicle loads. *Comput Struct*. 2015;157:76-88.
34. Pau A, Vestroni F. Train-weight-in-motion identification measuring time-histories of rail strains. *Proceedings of Eurodyn*. Athens, Greece; 23–26 November 2020.
35. Pau A, Vestroni F, Duca E, Platini M. Identification of freight train loads using time-histories of rail strains, 12th World Congress on Railway Research, Tokyo, Japan, 2019.
36. Sorenson HW. *Parameter Estimation: Principles and Problems*. New York: Marcel Dekker Inc.; 1980.

37. Beck JL, Katafygiotis LS. Updating models and their uncertainties. I: Bayesian statistical framework. *J Eng Mech-ASCE*. 1998;124(4): 455-461.
38. Goller B, Schuëller GI. Investigation of model uncertainties in Bayesian structural model updating. *J Sound Vib*. 2011;330(25):6122-6136.
39. Capecchi D, Vestroni F. Identification of finite element models in structural dynamics. *Eng Struct*. 1993;15(1):21-30.
40. Valikhani M, Younesian D. Bayesian framework for simultaneous input/state estimation in structural and mechanical systems. *Struct Control Health*. 2019;26(9):e2379.

How to cite this article: Pau A, Vestroni F. Weigh-in-motion of train loads based on measurements of rail strains. *Struct Control Health Monit*. 2021;e2818. https://doi.org/10.1002/stc.2818